applied mechanics

MDPI

Article

Static Analysis Method and Structural Optimization of Box-Type Subgrade for High-Speed Railways

Jianfeng Fang [1], Gentian Hong [1], Xin Wen [2,*], Runmin Wang [2], Qiang Shentu [1], Tao Chen [2] and Weichao Li [2]

[1] Hangzhou Railway Hub Engineering Construction Headquarters, China Railway Shanghai Group Co., Ltd., Hangzhou 315000, China; 649515359@qq.com (J.F.)
[2] College of Civil Engineering, Tongji University, Shanghai 200092, China; t.chen@tongji.edu.cn (T.C.); weichaoli@tongji.edu.cn (W.L.)
* Correspondence: 2430778@tongji.edu.cn

Abstract

A method based on a statically indeterminate planar frame model was developed for the analysis and evaluation of box-type subgrade structures in high-speed railways. The objective of this study is to establish a concise and mechanically rigorous framework capable of quantifying the effects of key geometric parameters on bending moments, shear forces, and slab deflection, thereby providing guidance for structural refinement. Symbolic derivation and structural mechanics theory are combined to formulate the analytical model, and finite element simulations in Abaqus are used to verify the theoretical predictions under the design loads of the Quzhou–Lishui railway section located between Quzhou City and Lishui City in Zhejiang Province, China. Key findings show the maximum bending moments at the slab center and web-slab junction, reaching 14,818 kN·m, and the maximum shear forces of 16,934 kN at the web-slab junction. The top slab center showed the maximum deflection, approximately 7.5×10^{-2} mm. Simulation errors were below 5%. The optimization results recommend a web spacing of 4.5–5 m and a web height of 5–8 m. In an engineering case, reducing the web spacing from 6 m to 5 m and adjusting the web height from 7 m to 6.5 m dropped the top-slab mid-span bending moment from 10,628 kN·m to 5603 kN·m (an 89.7% reduction). Concrete use fell by 2.61% (from 24,900 to 24,250 m^3/km), and overall costs dropped by about 5%. These findings demonstrate that the proposed analytical method provides an effective basis for rational parameter selection and preliminary structural design of box-type railway subgrades.

Keywords: box-type subgrade structure; structural mechanics; hyperstatic plane frame; finite element simulation

check for updates

Received: 14 October 2025
Revised: 14 November 2025
Accepted: 27 November 2025
Published: 3 December 2025

Citation: Fang, J.; Hong, G.; Wen, X.; Wang, R.; Shentu, Q.; Chen, T.; Li, W. Static Analysis Method and Structural Optimization of Box-Type Subgrade for High-Speed Railways. *Appl. Mech.* **2025**, *6*, 85. https://doi.org/10.3390/applmech6040085

Copyright: © 2025 by the authors. Licensee MDPI, Basel, Switzerland. This article is an open access article distributed under the terms and conditions of the Creative Commons Attribution (CC BY) license (https://creativecommons.org/licenses/by/4.0/).

1. Introduction

With the rapid development of high-speed railways, there are still some technical difficulties in the field of railway subgrades. To ensure high-quality train operation and smooth performance, railway subgrade engineering should have high strength, minimal settlement and excellent stability. However, when railways are constructed on soft foundation, the combined action of fill weight and train load may cause uneven settlement and stability problems, which significantly affects the operational safety of the track [1–3].

When designing and constructing railway subgrade projects, it is crucial to adopt practical engineering measures to ensure that the foundation's settlement and stability meet the required project standards [4–6]. Therefore, it is particularly important to develop and optimize new subgrade structures suitable for special geological conditions [7–14]. These

new subgrade structures have gradually become one of the feasible solutions to solve the related problems due to their comprehensive technical and economic advantages.

As a representative form of innovative subgrade design, the box-type subgrade structure has the advantages of small footprint, no requirement for traditional fill materials, high strength and integrity, and enhanced overall stiffness. In recent years, the research on the mechanical characteristics of box-type subgrade structure has made remarkable progress, and the vibration and noise characteristics are key indicators of long-term service performance. Li [15] revealed the sensitivity of box height, cover thickness, and longitudinal length to dynamic response based on a three-dimensional numerical model, and confirmed that the natural frequency of the box-type structure is much higher than the train excitation frequency. Zhu [16] demonstrated the internal force distribution law of the box-type structure by numerical simulation; Chen et al. [17] proposed an innovative analytical approach by decomposing the box into a plane rigid frame and an elastic foundation beam, thereby revealing the mechanism of the influence of foundation differential settlement on internal force distribution; Liu et al. [18] conducted an optimization study on haunches in box-type subgrades, found that haunch angles between 45° and 60° could reduce stress concentration at joints by up to 37.8%, providing quantitative guidance for local structural design. In addition, the refined simulation method of concrete box temperature field and early-age thermal stress by Zhang et al. [19] also provides valuable cross-disciplinary insights into the material performance of box-type subgrades. A number of studies have systematically evaluated the mechanical responses of box-type subgrades under different structural configurations and design parameters [20–23]. Chen et al. [24] applied a multi-objective optimization method based on genetic algorithms to determine the most economical configuration of box-type subgrade parameters, achieving notable reductions in material usage and construction costs. Liu et al. [25] utilized numerical simulation methods to study the shoulder augmentation method for concrete box subgrades, optimizing their structural forms. Although existing research has made breakthroughs in static simulation and local parameter evaluation, it still has two limitations: Firstly, static analysis mostly relies on three-dimensional finite element simulation or simplified local component models, with a lack of generalized two-dimensional symbolic models grounded in structural mechanics, which leads to insufficient engineering applicability of the sensitivity analysis of design parameters; secondly, the optimization research focuses on a single variable (such as haunch angle or cover thickness), without establishing a coupled mechanism between web spacing and structural height. To address the above bottlenecks, this study develops a two-dimensional symbolic analytical framework based on the displacement method in structural mechanics [26], formulated as a statically indeterminate planar frame model. This framework transforms the complex interactions among the top slab, webs, and foundation into a parameterized mechanical chain, enabling analytical solutions under various combinations of web spacing and height.

An engineering case of the Quzhou–Lishui Railway is used to implement a two-variable optimization of web parameters, revealing that coordinated optimization of web spacing and height can significantly improve the distribution of bending moment and shear force in the top slab. Through the verifications of structural mechanics analysis and finite element simulation, this paper provides a practical solution for the precise design of box-type subgrades.

2. Computational Analysis of Box-Type Subgrade Structures

2.1. Loading Conditions

The cross-sectional configuration of the box-type subgrade structure is illustrated in Figure 1. From top to bottom, the system consists of the rails: the track slab (1) that

anchors the rails; a ballast layer with lateral confinement (3); the reinforced concrete box structure (4); a cushion layer (5); and the foundation (6) at the bottom. Additionally, the structure is subjected to loads from roadside ancillary facilities on both sides (2). This integrated system is designed to effectively distribute and transmit train-induced loads.

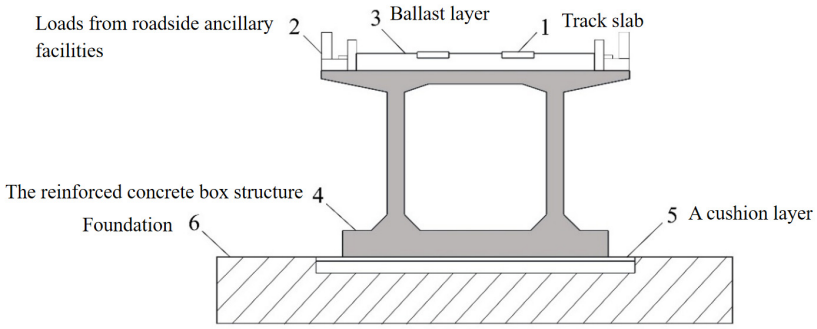

Figure 1. Schematic cross-section of the box-type subgrade structure.

The specific dimensions of this box-type subgrade structure are as follows: The concrete is designed to a strength grade of C45 according to the Chinese specification (GB 50010-2010 [27]), a total length of 39.96 m, a top slab width of 11.6 m, and a bottom slab width of 10.0 m. The clear spacing between the webs is 5.35 m, with a top slab thickness of 0.5 m, web thickness of 0.65 m, and bottom slab thickness of 1.0 m.

When considered as a whole, the structure is primarily subjected to its self-weight, the structural loads from components like the overlying track slab, and train loads. For the box-type subgrade structure, it can be simplified as a plane rigid frame structure for calculation, which is subjected to gravitational loading, lateral loads from surface-mounted facilities on both sides of the ballast, and vertical distributed loads transferred from the train to the ballast layer.

Based on this assumption, the structure is further idealized as a planar frame and analyzed as a plane strain problem, as illustrated in Figure 2. To ensure the generality of the theoretical formulation, all variable parameters are represented symbolically using letters.

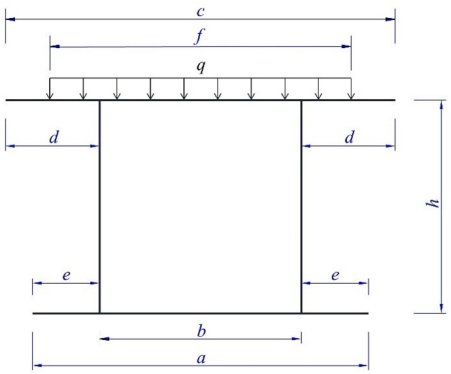

Figure 2. Simplified cross-sectional stresses diagram of box-type roadbed subgrade structure.

In the simplified model, the concrete members were assumed to be C45 concrete. The elastic modulus E was taken as 3.35×10^{10} Pa, the Poisson's ratio v was 0.2, and the density ρ was 2600 kg/m^3.

2.2. Model Assumptions and Simplification Basis

To enable the efficient mechanical analysis of box-type subgrade structure, this study adopts key assumptions and simplification rules, and the theoretical rationale and practical engineering background are described as follows:

(1) Structural continuity assumption: It is assumed that the box-type subgrade has strict continuity and uniformity along the longitudinal direction, and the internal force distribution of any cross-section can represent the overall structural response.
(2) Load dominance assumption: Only the fully loaded train condition is considered (equivalent linear load q = 5644.79 N/m), and loads from ballast layer appendages (accounting for <8%) are neglected.
(3) Material Constitutive Simplification: Concrete is modeled as a linear elastic material.
(4) Parametric Generalization: All geometric parameters (like web spacing b and height h) and load parameters (q) are expressed symbolically. Their physical interpretations are shown in Table 1, ensuring the model is applicable to different design scenarios.

Table 1. Symbolic parameter definition.

Symbol	Physical Interpretation	Unit
a	bottom slab width	m
b	clear distance between webs	m
c	top slab width	m
d	overhang length of the top plate flange	m
e	overhang length of the bottom slab flange	m
h	web-slab height	m
f	equivalent linear load width	m
q	equivalent linear load intensity	N/m

2.3. Mechanical Model for Box-Type Subgrade Structure

As illustrated in the simplified cross-sectional force analysis diagram of the box-type subgrade structure (Figure 3), the bottom slab width is a, with bottom flanges extending e on each side. The top slab width is c, with top flanges extending d on each side, and the web-slab height is denoted as h. The structure is analyzed as a statically indeterminate planar system under a uniformly distributed vertical load, represented by an equivalent linear load q with a width f, simulating a fully loaded train. The shear force, bending moment, axial force, strain, and displacement are derived accordingly. Since the bottom slab is connected to CFG piles embedded in the foundation, the bottom constraint is idealized as fully fixed in the analysis. Furthermore, the structural force-simplified diagram is shown in Figure 3, with auxiliary points as A, B, C, D, E, F, and G.

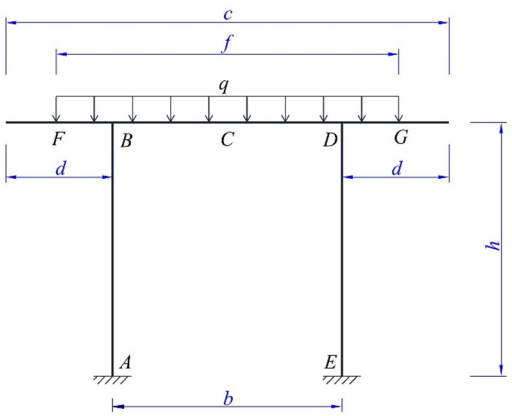

Figure 3. Simplified force diagram of box-type subgrade structure.

2.4. Structural Bending Moment Calculation and Diagram

Due to the structural symmetry, half of the structure is analyzed. A vertical section is made at the mid-span point C of the top slab, where there is vertical displacement, but no rotation. Therefore, a sliding support is used instead, and the left half of the structure is

analyzed. In this simplified model, the structural height is h, the length of the top flange remains d, and the equivalent linear load acts over the length of the top flange is $\frac{f-b}{2}$, as illustrated in Figure 4a.

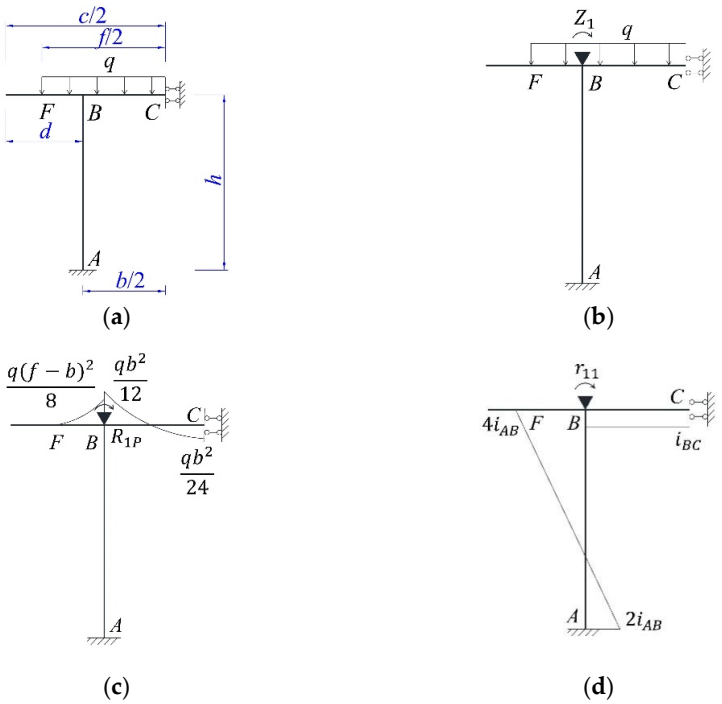

Figure 4. Bending moment calculation diagram: (**a**) Simplified half-structure model and applied equivalent load; (**b**) Basic structure in the displacement method with the introduced primary unknown; (**c**) Bending moment diagram under actual loading condition; (**d**) Bending moment diagram due to a unit rotational displacement at point B.

For this half-structure, the displacement method in structural mechanics is employed to calculate the internal bending moments [26]. First, determine the basic unknowns and establish the basic structure. In this case, the only primary unknown is the rotational displacement at point B. Add an additional constraint at point B and denote the parameter as Z1. The basic structure of the displacement method is shown in Figure 4b.

In the process of applying the displacement method, the rotational displacement equation (Long et al., 2000) [26] is introduced to form a closed analytical system. Since there is only one primary unknown, the displacement method yields the following governing equation:

$$r_{11}Z_1 + R_{1P} = 0, \tag{1}$$

where $\boldsymbol{r_{11}}$ is the coefficient; $\boldsymbol{Z_1}$ is the rotational displacement at point B; and $\boldsymbol{R_{1P}}$ is the free term.

The bending moment diagram under the actual loading condition (Figure 4c) and the moment diagram resulting from a unit rotational displacement at point B (Figure 4d) are shown accordingly.

For Figure 4c ($\boldsymbol{M_P}$), based on the moment equilibrium at point B, the following equation can be obtained:

$$\mathrm{R}_{1P} = \frac{\mathrm{q(f-b)}^2}{8} - \frac{\mathrm{qb}^2}{12}, \tag{2}$$

Conducting the numerical analysis of R_{1P}, considering practical conditions, the width of the ballast layer is generally no more than twice the width of the box structure, which means

$$\mathrm{f-b} < \mathrm{b}, \tag{3}$$

Therefore, R_{1P} is determined to be negative.

For Figure 4d ($\overline{M}$), according to the moment balance about point B, we can get

$$r_{11} = 4i_{AB} + i_{BC}, \tag{4}$$

Since the entire structure uses concrete of the same strength grade, it can be assumed that the elastic modulus of members AB and BC in the simplified force analysis diagram is E, and the section moment of inertia is denoted as $\boldsymbol{I_{AB}}$ for member AB and $\boldsymbol{I_{BC}}$ for member BC, then the following relationship holds

$$i_{AB} = \frac{EI_{AB}}{h}, \tag{5}$$

$$i_{BC} = \frac{EI_{BC}}{b/2}, \tag{6}$$

Substituting Equations (5) and (6) into Equation (4) yields

$$r_{11} = 4i_{AB} + i_{BC} = \frac{4EI_{AB}}{h} + \frac{2EI_{BC}}{b}, \tag{7}$$

Substituting Equations (2) and (7) into Equation (1) yields

$$Z_1 = -\frac{R_{1P}}{r_{11}} = \frac{\frac{qb^2}{12} - \frac{q(f-b)^2}{8}}{\frac{4EI_{AB}}{h} + \frac{2EI_{BC}}{b}}, \tag{8}$$

It can be seen that the value of $\boldsymbol{Z_1}$ is greater than 0, so the original direction assumption of $\boldsymbol{Z_1}$ is positive. Based on the principle of superposition,

$$M = \overline{M} \cdot Z_1 + M_P, \tag{9}$$

The bending moment diagram of the original half structure can thus be obtained. By symmetry, the bending moment diagram for the full simplified structure is shown in Figure 5.

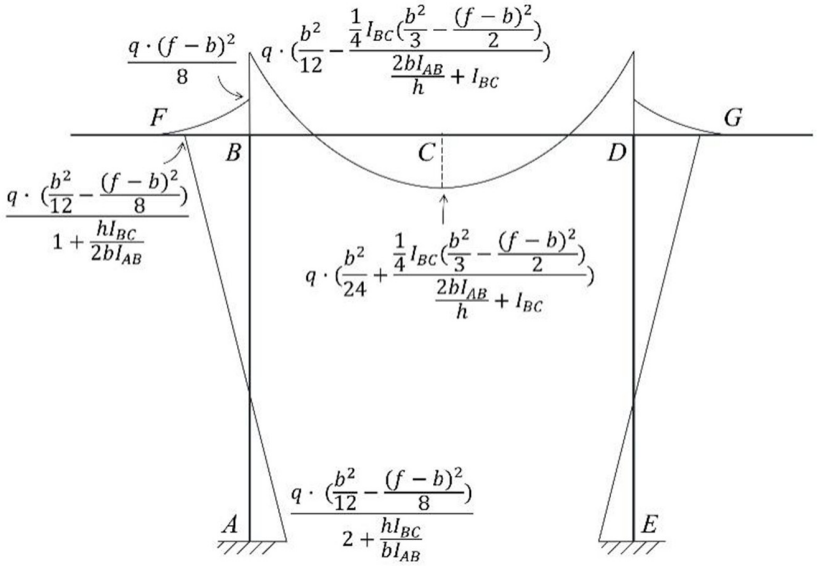

Figure 5. Bending moment diagram of the overall structure (symmetric left and right).

2.5. Structural Shear Force Calculation and Diagram

Based on the member equilibrium method in structural mechanics, the shear force diagram is derived from the bending moment diagram.

Using moment equilibrium and force equilibrium methods, the shear forces on the members are directly calculated, and the overall shear force diagram is shown in Figure 6.

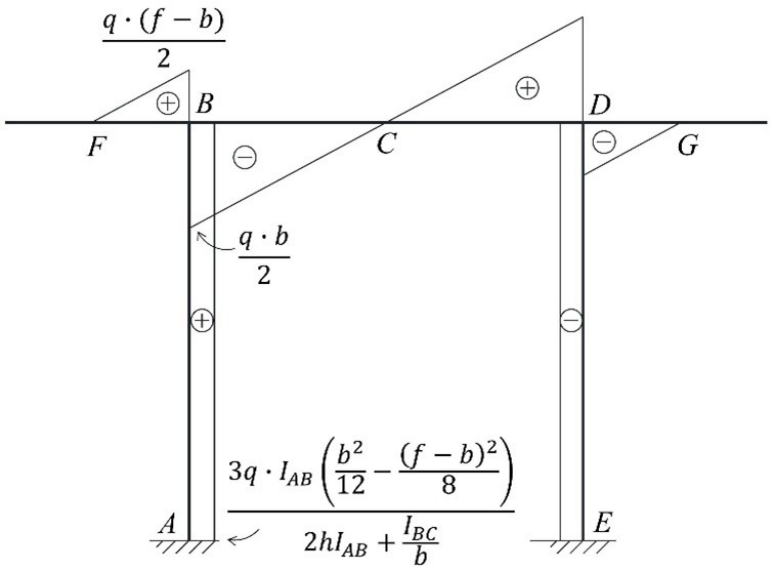

Figure 6. Overall shear force diagram (symmetric left and right).

2.6. Structural Deformation Analysis and Maximum Deflection of the Top Slab

Based on the bending moment diagram shown in Figure 5, the deformation shape of the structure under the applied train load is illustrated in Figure 7.

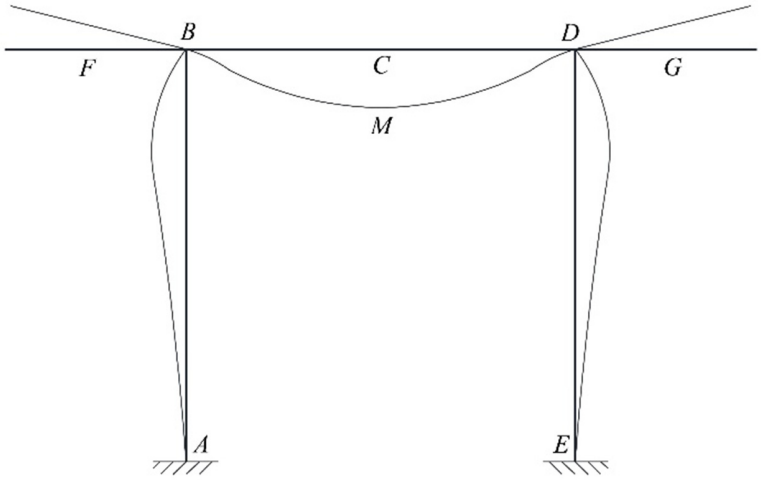

Figure 7. Overall structural deformation diagram.

Determining the maximum deformation of the top slab of the box-type subgrade structure under static train loading is of significant engineering value. Therefore, the maximum deflection at point M, located at the midspan of member BD in the simplified structural system (shown in Figure 7) is required.

To calculate the deflection at point M, the displacement method from structural mechanics is also used. However, in contrast to the structural simplification used for moment analysis, the BC member is considered as a beam fixed at both ends, with point C treated as a fixed support. Similarly, the left half of the structure is analyzed, resulting in the simplified half-structure, as shown in Figure 8a.

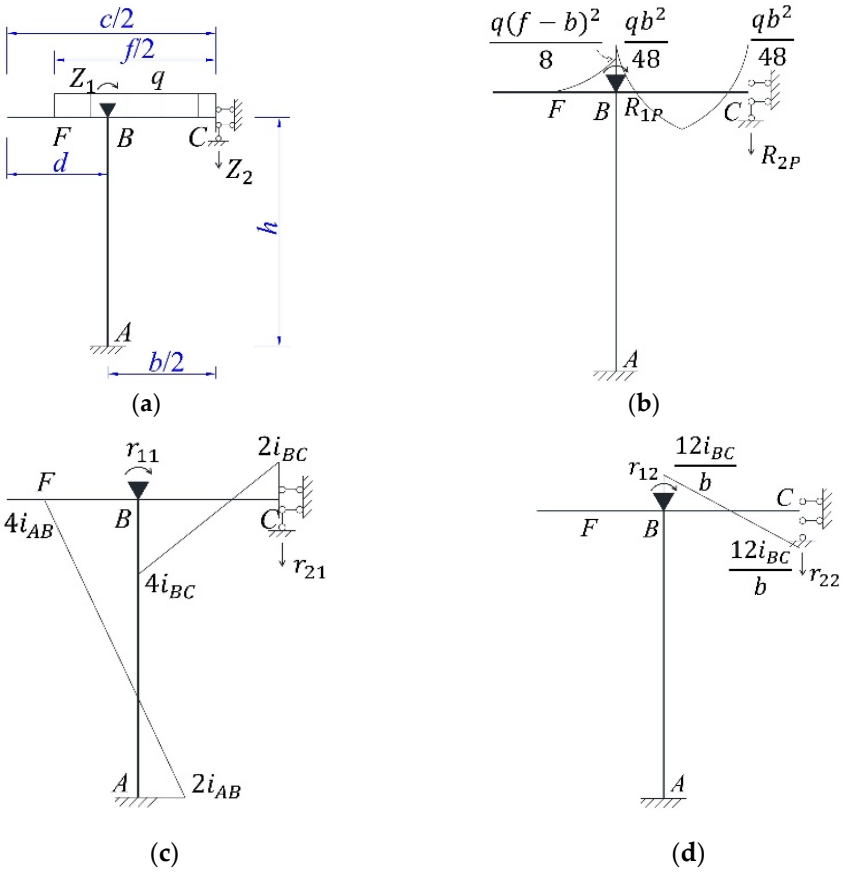

Figure 8. Calculation diagram of maximum deformation of the top slab: (**a**) Simplified half-structure used for deflection analysis, with BC treated as a fixed–fixed beam; (**b**) Bending moment diagram under the actual load M_P; (**c**) Bending moment diagram induced by a unit rotational displacement at point B $\overline{M}_1$; (**d**) Bending moment diagram induced by a unit vertical displacement at point C $\overline{M}_2$.

With two primary unknowns, the typical equation of displacement method can be listed as

$$r_{11}Z_1 + r_{12}Z_2 + R_{1P} = 0, \tag{10}$$

$$r_{21}Z_1 + r_{22}Z_2 + R_{2P} = 0, \tag{11}$$

where $\boldsymbol{r_{11}}$, $\boldsymbol{r_{12}}$, $\boldsymbol{r_{21}}$, $\boldsymbol{r_{22}}$ are the coefficients; $\boldsymbol{Z_1}$ is the rotational displacement at point B; $\boldsymbol{Z_2}$ is the vertical displacement at point C; and $\boldsymbol{R_{1P}}$, $\boldsymbol{R_{2P}}$ are free terms.

The bending moment diagram resulting from the actual load ($\boldsymbol{M_P}$) is presented in Figure 8b, that induced by a unit rotational displacement at point B ($\overline{\boldsymbol{M_1}}$) is shown in Figure 8c, and that induced by a unit vertical displacement at point C ($\overline{\boldsymbol{M_2}}$) is illustrated in Figure 8d.

Based on the moment equilibrium, the following can be obtained from Figure 8b ($\boldsymbol{M_P}$):

$$R_{1P} = \frac{q(f-b)^2}{8} - \frac{qb^2}{48}, \tag{12}$$

$$R_{2P} = -\frac{qb}{4}, \tag{13}$$

The following results can be obtained from Figure 8c ($\overline{\boldsymbol{M_1}}$):

$$r_{11} = 4i_{AB} + 4i_{BC} = \frac{4EI_{AB}}{h} + \frac{8EI_{BC}}{b}, \tag{14}$$

$$r_{21} = -\frac{12i_{BC}}{b} = \frac{24EI_{BC}}{b^2}, \tag{15}$$

And the results derived from Figure 8d ($\overline{M_2}$) are as follows:

$$r_{12} = -\frac{12i_{BC}}{b} = \frac{24EI_{BC}}{b^2}, \tag{16}$$

$$r_{22} = \frac{48i_{BC}}{b^2} = \frac{96EI_{BC}}{b^3}, \tag{17}$$

Substituting Equations (12)–(17) into Equations (10) and (11), we obtain the typical equations of the displacement method:

$$(\frac{4EI_{AB}}{h} + \frac{8EI_{BC}}{b})\cdot Z_1 + \frac{24EI_{BC}}{b^2}\cdot Z_2 + \frac{q(f-b)^2}{8} - \frac{qb^2}{48} = 0, \tag{18}$$

$$\frac{24EI_{BC}}{b^2}\cdot Z_1 + \frac{96EI_{BC}}{b^3}\cdot Z_2 - \frac{qb}{4} = 0, \tag{19}$$

Now the typical system of equations contains only two unknowns, and two equations, making it solvable. The result $\boldsymbol{Z_2}$ is the deflection at point C, which is the maximum deformation of the top slab of box-type subgrade structure in actual engineering when subjected to a static train load.

3. Engineering Case Analysis

For the demonstration section of the newly constructed Quzhou–Lishui Railway box-type subgrade structure, the corresponding engineering parameters are incorporated into the established mechanical model to calculate the maximum bending moment, shear force, and deflection under actual static train loads. This facilitates a more comprehensive theoretical assessment for the structural safety of the demonstration section.

3.1. Structural Parameters of the Box-Type Subgrade

3.1.1. Geometric Parameters

Since the box-type subgrade structure features has plate thickness, while the simplified two-dimensional analytical model adopts zero-thickness beam elements, the dimensional reduction is conducted based on centerline-to-centerline distances between slabs [28]. The thickness of the simplified structure is taken as a unit thickness of 0.1 m. The original structural dimension and the corresponding simplified model are shown in Figures 9 and 10.

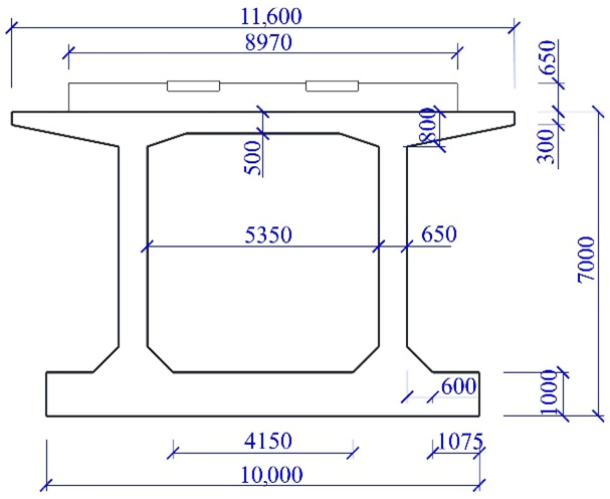

Figure 9. Dimensional diagram of the original box-type subgrade structure.

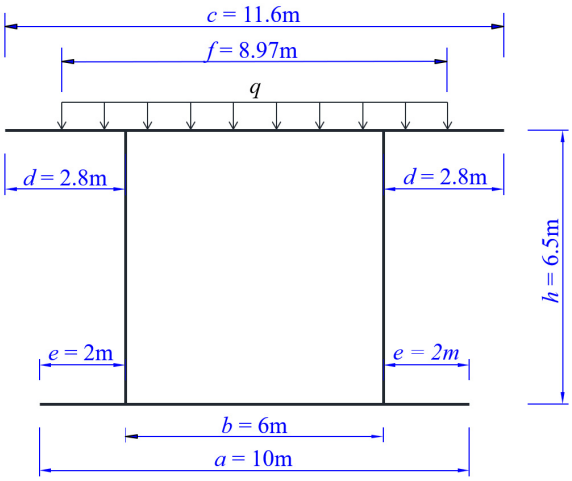

Figure 10. Dimensional diagram of the simplified structural model.

3.1.2. Section Moment of Inertia

As the calculation of the bending moment diagram requires the section moments of inertia ($\boldsymbol{I_{AB}}$ and $\boldsymbol{I_{BC}}$), the moments of inertia for members AB and BC in the simplified model must be explicitly evaluated:

$$\mathrm{I_{AB}} = \frac{\mathrm{bh}^3}{12} = 0.00229\ \mathrm{m}^4, \tag{20}$$

$$I_{BC} = \frac{bh^3}{12} = 0.00104\ m^4, \tag{21}$$

3.1.3. Static Load Parameters

The high-speed train under full load is selected as the static load. Typically, an 8-car trainset has a length of approximately 200 m, while a 16-car trainset extends to about 400 m. The overall length of a high-speed train mainly depends on the number of cars and the length of each car, which is generally around 25 m [29].

The tare weight refers to the total weight of the high-speed trainset, which means the weight of the train when empty. It is typically expressed in ton and varies significantly among different train models. For example, the tare weight of a CRH2 trainset ranges from 41.5 t to 48 t, while that of a CRH3 trainset ranges from 50.38 t to 54.69 t [30].

A relatively large safety factor was used in the calculation, and the mass under full-load conditions is defined as 60 tons per car. Therefore, the load borne by a 9.97 m long track slab is calculated as 23.928 t, corresponding to an equivalent force of 234,494.4 N. Based on the ballast dimension of the box-type subgrade structure, the contact area is 89.4309 m^2, resulting in a pressure of 2622.07 $\frac{\mathrm{N}}{\mathrm{m}^2}(\mathrm{Pa})$. This pressure can then be converted into an equivalent linear load of 5644.79 N/m.

3.2. Calculation Results

Based on the aforementioned calculation, the bending moment, shear force, and the maximum mid-span deflection of the top slab at various positions of the simplified structure can be obtained under the static load of a fully loaded train. The resulting bending moment diagram is shown in Figure 11, and the shear force diagram is presented in Figure 12.

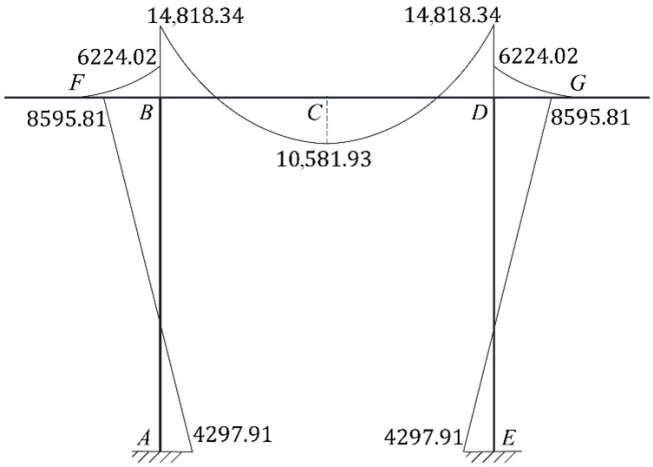

Figure 11. Calculated bending moment diagram of the simplified structure in the demonstration.

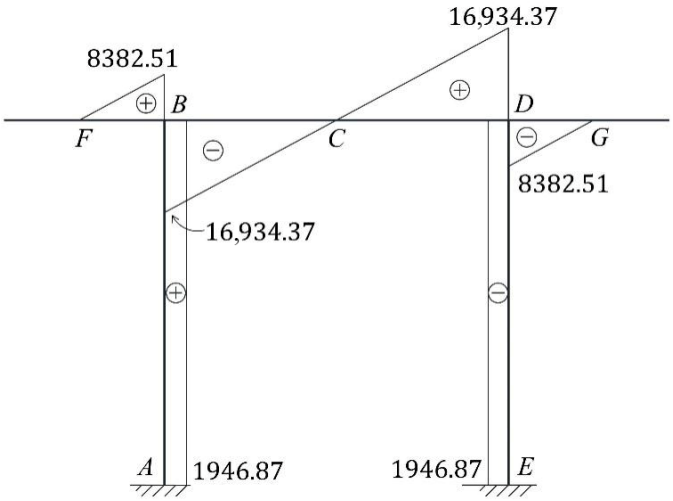

Figure 12. Calculated shear force diagram of the simplified structure in the demonstration section.

4. Two-Dimensional Numerical Simulation of Structure and Result Comparison

4.1. Finite Element (FE) Model Establishment

4.1.1. Material Model Selection

In finite element analysis, the selection of material model has a significant impact on the accuracy of the numerical simulation results. Choosing a suitable material model is a key prerequisite for ensuring the reliability of the simulation outcomes. Based on the engineering material parameters presented in Section 2.1, the simplified concrete members are modeled using C45 concrete [27].

4.1.2. Determination of Numerical Simulation Parameters

(1) Model dimension
To enable a rigorous comparison with the theoretical calculation results, the cross-sectional simplification of the FE model follows the box-type subgrade structural parameters given in Section 2.1, with the thickness set to a unit value of 0.1 m, consistent with the theoretical calculation.

(2) Cross-sectional dimension
For the moment of inertia of members in the simplified two-dimensional box-type subgrade structure, the dimensions are determined based on the actual engineering configuration. The web members on the left and right sides are modeled as rectangular

sections with a width of 0.1 m and a height of 0.65 m, while the top slab members are modeled as rectangular sections with a width of 0.1 m and a height of 0.5 m.

(3) Load components
For the upper line load of the numerical simulation, the value q is taken as 5644.79 N/m according to the calculation in Section 3.1, and the direction is vertically downward.

The overall FE numerical model is shown in Figure 3.

4.2. Comparative Analysis of Numerical Simulation Results

4.2.1. Two-Dimensional Simplified FE Model of Box-Type Subgrade Structure

To analyze the two-dimensional FE model of the box-type subgrade, a simplified geometry, described in Section 3.1, was implemented in ABAQUS. The concrete members were idealized using two-node linear beam elements (B21) [31,32]. As result of the sensitivity study for mesh size, a mesh size of about 0.05 m was suggested in this study, with local refinement at the web–slab junctions (nodes B and D) to 0.02 m. The mesh convergence verification confirmed that the maximum error in bending moment was less than 1%.

The Static General analysis step was used, with an initial incremental step of 1, a maximum of 100 increments, and a maximum of 1 iteration per increment. The residual force tolerance was set to 1×10^{-5}. The linear load q was adopted based on the parameters calculated in Section 3.1. The loading position was selected based on the box-type structure parameters of the reference demonstration section, applied vertically downward on the top slab, with the ends terminating at the junction between the ballast and the partition.

Since the box-type subgrade structure is uniform along the railway at any cross-section, the analysis of the simplified two-dimensional model can be regarded as a plane strain problem. Moreover, as there is no lateral support on either side of the web plate in the actual structure, its edges are modeled as free boundaries to simulate the real condition of no lateral restraint. Considering that the concrete at the bottom of structure is integrally cast with the CFG (Cement–Fly ash–Gravel) pile caps, it can be regarded as a consolidated constraint under static loading. Therefore, fixed constraints (U1 = U2 = UR3 = 0) are applied to the nodes at the underside of the slab. The loading and boundary conditions of the FE model are illustrated in Figure 13.

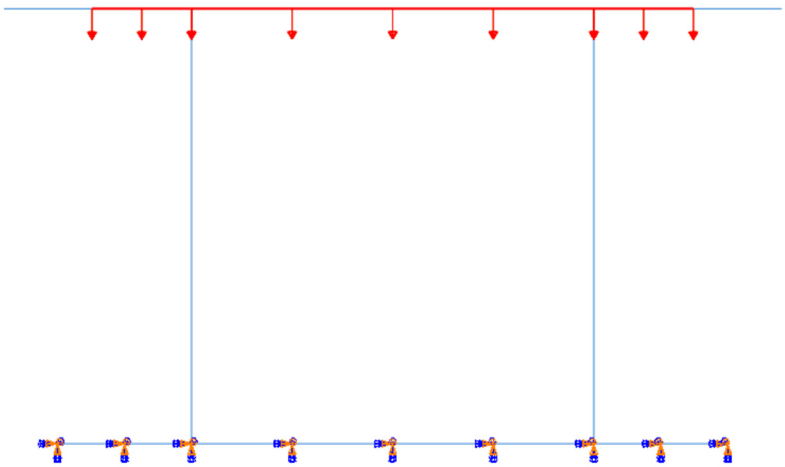

Figure 13. Loading and boundary constraints of FE model.

4.2.2. Calculation and Analysis of the Simplified Two-Dimensional Model

In processing the FE calculation results, the main consideration is to compare the structural bending moment, shear force and maximum mid-span deflection of the top slab of the box-type subgrade structure under static load with the theoretical analysis.

(1) Bending Moment Analysis

Figure 14 presents the bending moment contour plot for the simplified 2D model of the box-type subgrade structure. As shown, the maximum negative bending moment occurs at the mid-span of the top slab, while additional negative moments are observed on the outer side of the top slab–web junction and the upper portion of the web plate. The maximum positive bending moment is located on the inside of the top plate at the junction with the web plate. The bending moment distribution is symmetric and is generally consistent with the typical distribution of bending moments in box-type subgrade structures under normal conditions, as described in Section 2.3 (Figure 5).

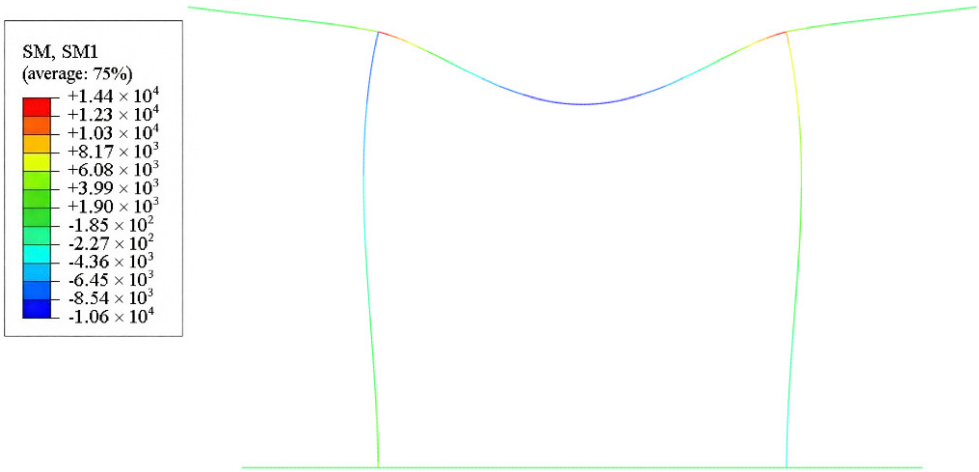

Figure 14. FE model bending moment contour plot.

Figure 15 shows a comparison of the FE simulation bending moment values with theoretical analysis using actual section data. It can be seen that the method in Section 2.2 for calculating the bending moment of box-type subgrade structures under train static load, which is applicable to arbitrary dimensions, exhibits good agreement with the simulation results and is suitable for preliminary theoretical analysis. A comparison and error analysis of the theoretical and simulated bending moment values at key locations of the top slab are presented in Table 2.

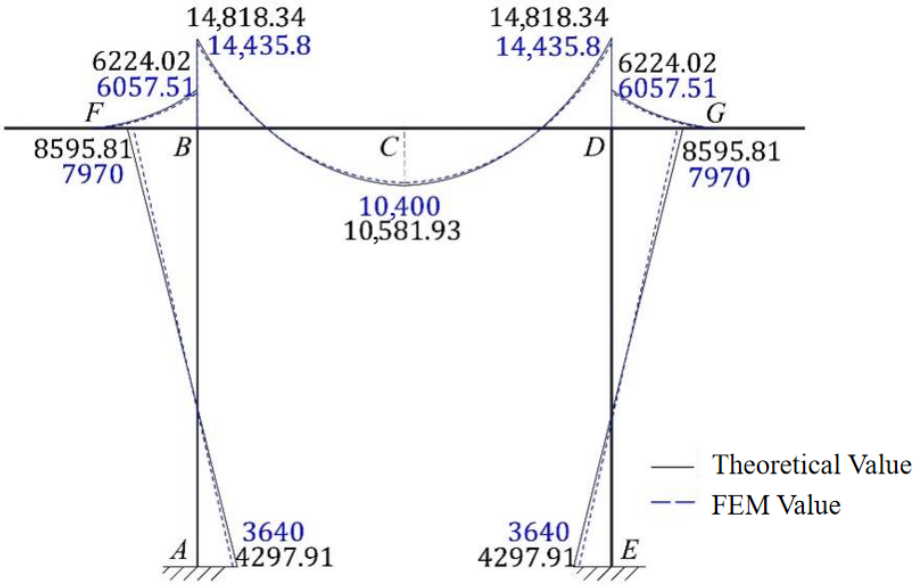

Figure 15. Comparison of bending moments between FE results and theoretical calculation.

Table 2. Bending moment comparison at key positions of the top slab.

Position	Theoretical Value (kN·m)	FEM Value (kN·m)	Error
Midpoint of Top Slab	10,581.93	10,400	1.75%
Inner Side of Web-Deck Joint	14,818.34	14,435.80	2.65%
Outer Side of Web-Deck Joint	6224.02	6057.51	2.75%

(2) Shear Force Analysis

Figure 16 presents the shear force contour plot of the simplified two-dimensional box-type subgrade structure. It can be observed that the shear forces on the top slab are concentrated within the loaded region, vary linearly, and exhibits a transition between positive and negative values at the interface between the web and top plates. The shear forces on the left and right webs are constant but opposite in sign. The overall shear force distribution from the FE model is consistent with the trend of the theoretical shear force diagram.

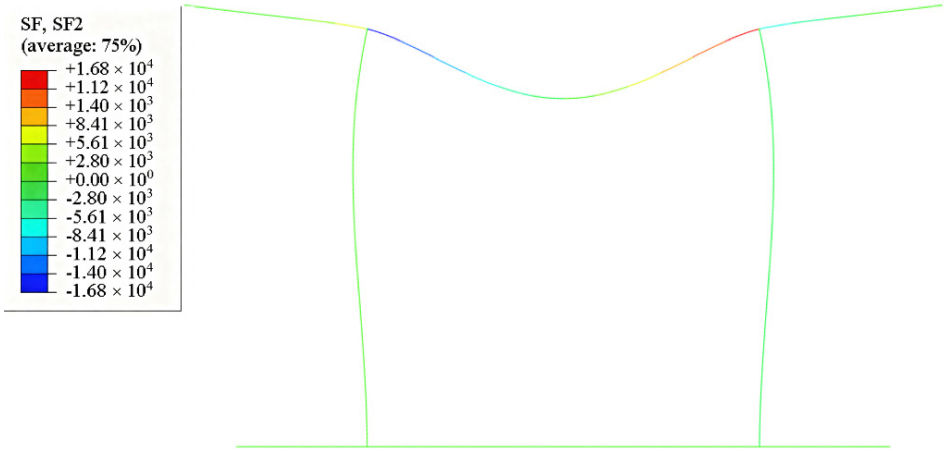

Figure 16. FE model shear force contour plot.

Figure 17 compares the FE simulation results with the theoretical analysis based on actual demonstration section data. Table 3 summarizes the comparison and error analysis of shear force values at critical locations between theoretical calculations and FE simulations.

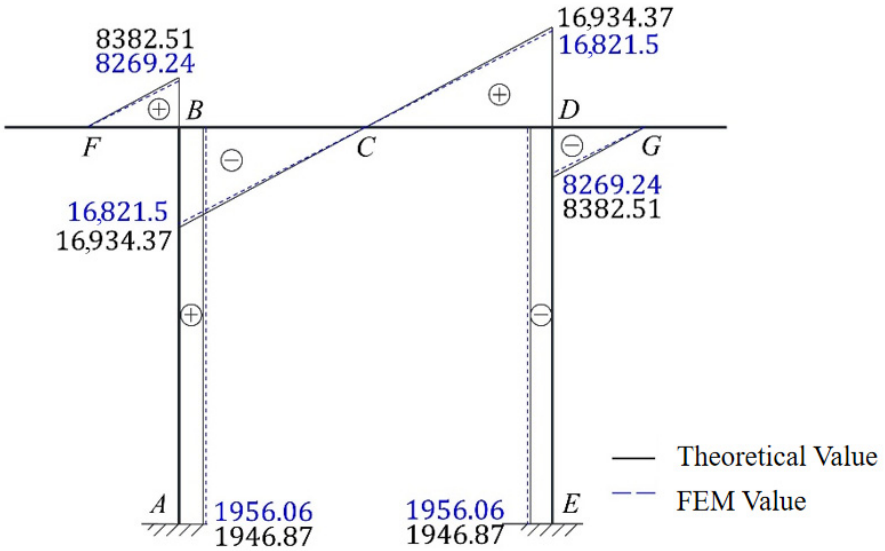

Figure 17. Comparison of shear force between FE results and theoretical calculation.

Table 3. Shear force comparison at key structural locations.

Location	Theoretical Value (kN)	FEM Value (kN)	Error
Inner side of web–top slab junction	16,934.37	16,821.5	0.67%
Outer side of web–top slab junction	8382.51	8269.24	1.34%
Web	1946.87	1956.06	0.47%

(3) Maximum Deformation Analysis

Figure 18 presents the displacement contour plot of the simplified two-dimensional box-type subgrade structure. It can be seen that, under this working condition, the maximum deformation occurs at the midpoint of the deck, with a deflection of 7.497×10^{-5} m. Compared with the theoretical calculation in Section 2.6, the overall deformation of the structure is basically consistent, and the maximum deflection values are nearly identical. This further validates the feasibility and accuracy of the theoretical calculation method introduced in this study for analyzing box-type subgrade structures under train static loads.

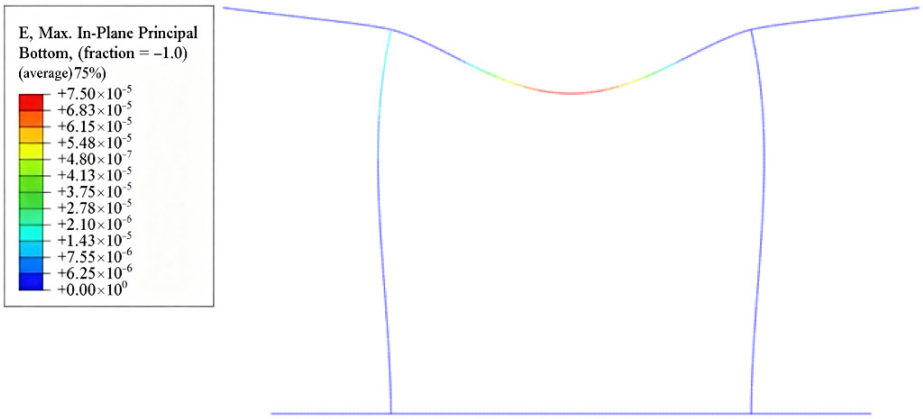

Figure 18. FEM displacement contour plot.

5. Parametric Analysis and Structural Selection

As analyzed in Section 2.1, the primary loads acting on the box-type subgrade structure are pavement loads, train loads, and the self-weight of the structure. Combining the bending moment distribution and displacement diagrams of the actual box-type subgrade structure shown in Figures 5 and 7, it is evident that the bending moments (absolute values) are relatively high at the mid-span of the top slab and the connections between the web plates and the top slab, and the vertical displacement at the mid-span of the top slab is also quite significant. In addition, the data in the figures indicate that the bending moments at the mid-span of the top slab, the junction between the web plates and the top slab, as well as within the web plates themselves, are influenced by the parameters: b (web spacing), h (web height), and f (the contact width between the load and the top slab), and f is the ballast width, which is not within the scope of the box-type subgrade structure selection in this study.

This section takes the bending moments at the mid-span of the top slab, the connection between the web plates and the top slab, and the maximum bending moment at the upper part of the web plates as key reference indicators, combines the changes in the spacing between the two webs and the web height to determine a more reasonable structural configuration. To simplify the analysis, this section is based on the engineering case presented in Section 3, employing the method of controlled variables while neglecting the effects of the thicknesses of the top slab, web plates, and bottom slab. In subsequent figures,

bending moments in each slab are defined as positive when the tensile stress occurs on the lower side.

5.1. Web Spacing

Figure 19 illustrates the variation in bending moments at key structural locations with changes in the web spacing, while all other conditions remain constant. The results indicate that, as the web spacing increases, the bending moments at the mid-span of the top slab and at the junction between the web and top slab show a gradually increasing trend, whereas the maximum absolute bending moment in the web first decreases and then increases. Therefore, in engineering design, considering the bending moments of both the web and the top slab, the bending moment performance of the structure is best when the web spacing is between 4.5 m and 5 m. However, it should be noted that the design complies with the code requirement limiting the span-to-thickness ratio of one-way reinforced concrete slabs to no more than 30 [27].

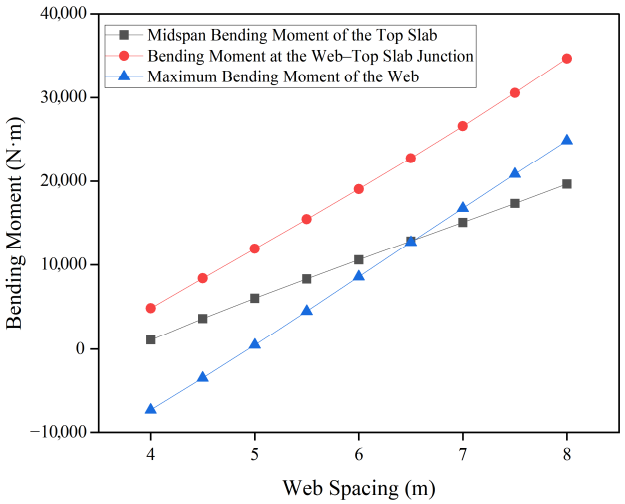

Figure 19. Effect of web spacing on the bending moments at key structural locations.

5.2. Web Height

Figure 20 shows the variation in bending moments at key locations with changes in web height, while keeping all other parameters constant. The parameter *t* can be seen that as web height increases, the bending moment values in the middle of the top slab and at the web–top slab junction gradually increase, as does the maximum bending moment in the web, with no significant changes in magnitude. Therefore, in engineering design, variations in web height within a moderate range do not significantly affect the overall structural safety. However, considering that the bending moment at the web–top slab junction is relatively large and tends to increase with greater web height, it is recommended that excessively large web heights be avoided. For the present case, the web height should be within the range of 5 m to 8 m.

5.3. Proposed Structural Selection Scheme

For the box-type subgrade structure with a height of 7 m and a web spacing of 6 m considered in Section 3, the parametric analysis in this section suggests adjusting the web height to 6.5 m and the web spacing to 5 m, thereby enhancing the structural strength while reducing construction costs. Finally, the selected structural configuration is shown in Figure 21. Through finite element simulation, the bending moment comparison at various locations of the top slab before adjustment (web height 7 m, web spacing 6 m) and after adjustment (web height 6.5 m, web spacing 5 m) is shown in Figure 22. The comparison results indicate that, the bending moment at the junction between the top slab and the web

decreased from 14,400 N·m to 12,800 N·m, representing a reduction of 11.1%. The bending moment at the midspan of the top slab decreased from −10,628.2 N·m to −5603.38 N·m, corresponding to a reduction of 89.7%.

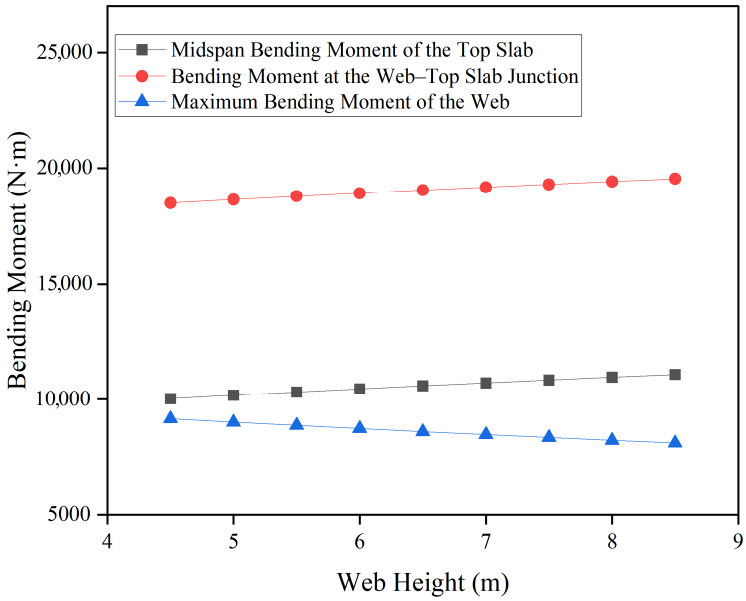

Figure 20. Effect of web height on the bending moments at key structural locations.

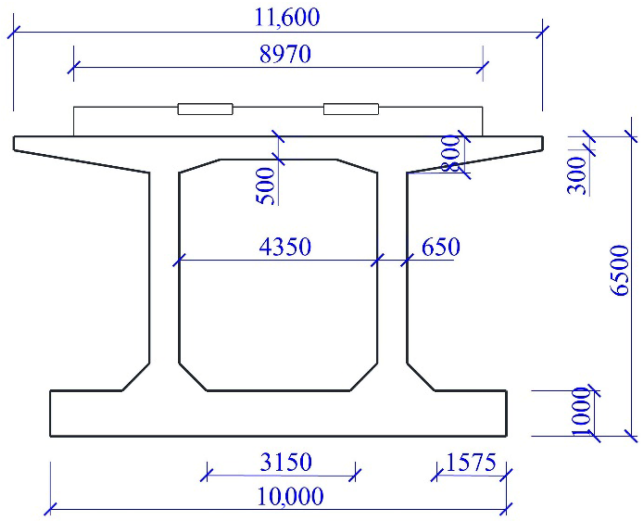

Figure 21. Selected design of the box-type subgrade structure for the engineering case (unit: m).

The economic analysis before and after structural adjustment is shown in Table 4. The proposed scheme—with a web spacing of 5 m and a web height of 6.5 m—reduces concrete consumption by 2.61% while ensuring structural safety. Considering the corresponding reduction in reinforcement demand due to changes in the concrete structure, as well as improved formwork utilization, the proposed scheme can lower construction costs by approximately 5%, which has notable economic benefits and engineering feasibility.

Table 4. Economic comparison of structural design schemes.

Parameter	Original Design	Selected Design	Percentage Change
Web Spacing (m)	6.0	5.0	−16.67%
Web Height (m)	7.0	6.5	−7.14%
Concrete Consumption per km (m^3)	24,900	24,250	−2.61%

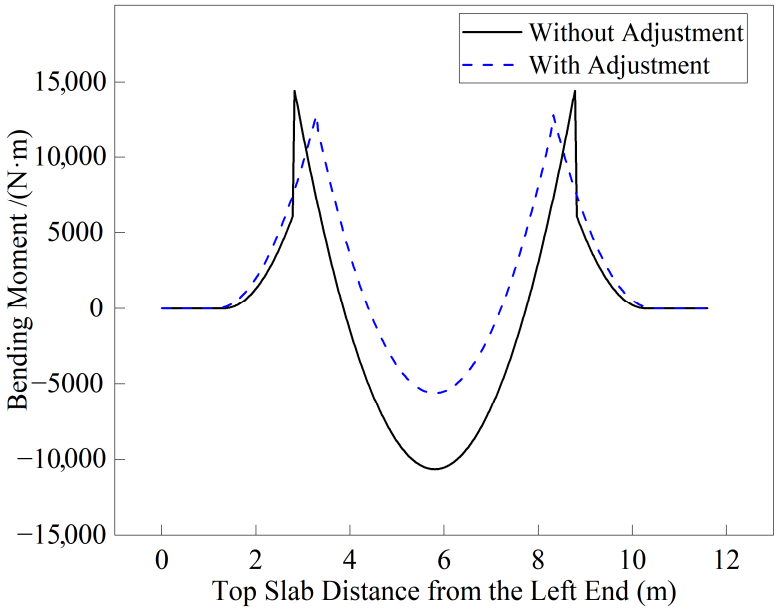

Figure 22. Comparison of top slab bending moments without and with adjustment.

6. Conclusions

(1) A symbolic modeling-based static analysis framework for a box-type subgrade structure was constructed. By simplifying the structure into a planar frame model and selecting key parameters such as web spacing (b), web height (h), and load (q) as symbolic variables, a universal symbolic solution system was established. Based on the structural symmetry, the displacement method was applied to the simplified half-structure to analyze bending moments, shear forces, and deformations resulting in symbolic expressions. The analysis shows that the actual internal forces under train loads exhibit clear regularity and consistency. This study focuses on the static response and parameter optimization of the box-type subgrade structure. Subsequent work will incorporate dynamic response analysis to further validate the long-term service performance of the optimized structure.

(2) Actual engineering verification and mechanical performance evaluation: Engineering verification based on the demonstration section of the newly constructed Quzhou–Lishui railway box-type subgrade shows that the maximum bending moment of the structure under train load in this section is approximately 14,818 kN·m, the maximum shear force is about 16,934 kN, and the deflection at the mid-span of the top slab is 7.5×10^{-2} mm. These analysis results provide a crucial theoretical basis for the design optimization and safety evaluation of the box-type subgrade structure.

(3) Verification of Theory-Simulation Consistency: A two-dimensional Abaqus FE model verified the analytical framework. The comparison shows a bending moment error of 1.75% at the midpoint of the top slab (10,400 vs. 10,582 kN·m), a peak shear force error of 0.67% (16,822 vs. 16,934 kN), and a deformation error of less than 0.5% (7.497×10^{-5} m vs. 7.5×10^{-5} m). These results confirm the reliability of the symbolic modeling method in practical engineering applications. The simulation model strictly adopts the theoretical calculation parameters from the engineering case (web clear spacing 6 m, top slab length 11.6 m, etc.), with boundary conditions and loading consistent with the theoretical model, ensuring that the validation outcomes provide valuable guidance for engineering practice.

(4) Structural Parametric Analysis and Structural Verification: Parametric sensitivity analysis indicates that the web spacing has a pronounced effect on the bending moment distribution. A web spacing of 4.5–5 m and a height of 5–8 m is recommended

to satisfy the span-to-thickness ratio specified in the code. After optimization (spacing reduced from 6 m to 5 m, height from 7 m to 6.5 m), the mid-span bending moment of the top slab decreased from 10,628 kN·m to 5603 kN·m (a reduction of 89.7%), while concrete consumption decreased by 2.61% (from 24,900 to 24,250 m^3/km), and the overall construction cost was saved by approximately 5%. The symbolic modeling system used in this study has generalizability, and the results provide a reference benchmark for projects with similar geological conditions and load levels, enabling rapid adaptation in practical design through symbolic parameter adjustment. Furthermore, the potential influence of top slab thickness on the structural response under accidental loads deserves attention and may be investigated in future studies as an auxiliary parameter.

Author Contributions: Conceptualization and methodology, J.F., Q.S. and G.H.; validation and formal analysis, T.C., W.L. and R.W.; data curation, J.F., Q.S. and G.H.; writing—original draft preparation, R.W. and X.W.; writing—review and editing, T.C. and W.L. All authors have read and agreed to the published version of the manuscript.

Funding: This research was funded by China Railway Shanghai Group Co., Ltd.: Research on Construction Technology of High-speed Railway Box-type Subgrade, grant number 2022156. The authors declare that this study received funding from China Railway Shanghai Group Co., Ltd. The funder had the following involvement with the study: conceptualization, methodology, and data curation.

Institutional Review Board Statement: Not applicable.

Informed Consent Statement: Not applicable.

Data Availability Statement: The original contributions presented in this study are included in the article.

Conflicts of Interest: Jianfeng Fang, Gentian Hong and Qiang Shentu are affiliated with Hangzhou Railway Hub Engineering Construction Headquarters, China Railway Shanghai Group Co., Ltd., China company. They declare that the research was conducted in the absence of any commercial or financial relationships that could be construed as a potential conflict of interest.

References

1. Yan, X.; Xu, G. Analysis of static effects of subgrade structure performance unevenness on ballastless track. *J. China Railw. Soc.* **2016**, *38*, 98–102.
2. Cui, X.; Yang, H.; Du, B.; Guo, G.; Zhang, B. Analysis of the impact of subgrade uneven settlement on damage and deformation of CRTSII slab ballastless track. *J. China Railw. Soc.* **2021**, *43*, 91–97.
3. Yang, Y. Research on non-uniform settlement control technology of high speed railway roadbed. *Railw. Constr. Technol.* **2013**, *4*, 47–51.
4. Liang, B.; Cai, Y. Dynamic analysis of high-speed railway subgrade under uneven conditions. *J. China Railw. Soc.* **1999**, *2*, 93–97.
5. Ye, Y.; Zhou, J. Discussion on the design of railway subgrade structure. *J. Railw. Eng. Soc.* **2005**, *1*, 39–46.
6. Bi, Z.; Ye, Y.; Cai, D.; Yan, H.; Ouyang, M.; Su, K. Research on high-speed railway subgrade design method based on energy dissipation and dynamic stability characteristics. *Appl. Sci.* **2025**, *15*, 734. [CrossRef]
7. Shaikh, M.F.; Nallasivam, K. Static analysis of box-girder bridge under the influence of Indian railway vehicle loading using ANSYS finite element model. *Adv. Bridge Eng.* **2022**, *3*, 25. [CrossRef]
8. Qi, Y.; Xiao, S. The railway quadra-pot-shape earthworks structure analysis method. *China Civ. Eng. J.* **2022**, *55*, 116–128.
9. Guo, S. Optimization analysis and research on cantilever U-shaped subgrade structure of high-speed railway. *Railw. Stand. Des.* **2022**, *67*, 1–6.
10. Xiao, Z.-W.; Zhang, Y. Finite Element Modeling and Seismic Response Analysis of Pile Slab Structure. In Proceedings of the 2020 International Conference on Intelligent Transportation, Big Data & Smart City, Vientiane, Laos, 11–12 January 2020; pp. 122–126. [CrossRef]
11. Wu, J.; Li, J. Research on the application of U-shaped structure in railway embankment section. *Railw. Stand. Des.* **2013**, *9*, 44–46.
12. Zhang, J. Research on the structure mechanism of pallet U-shaped subgrade. *Subgrade Eng.* **2012**, *4*, 118–122.

13. Wang, R.; Chen, T.; Li, W. Research and application status of concrete subgrade structure in high-speed railway. *Subgrade Eng.* **2024**, *4*, 18–26.
14. Leng, W.; Nie, R.; Yang, Q.; Zhao, C.; Mei, H. Preliminary study on structure and performance of new prestressed subgrade. *J. China Railw. Soc.* **2016**, *38*, 111–119.
15. Li, Y. Research on dynamic characteristics of box subgrade structure of high-speed railway. *Railw. Constr. Technol.* **2022**, *7*, 76–80.
16. Zhu, W. Research on Structural Performance of Box Subgrade in High Speed Railway. Ph.D. Thesis, Southwest Jiaotong University, Chengdu, China, 2021.
17. Chen, W.; Xiao, S.; Wang, X.; YU, L. Research on the static analysis method of railway box-type subgrade structure. *Railw. Stand. Des.* **2025**, *66*, 1–10.
18. Liu, J.; Liu, J.; Zhou, W.; Xia, B.; Zhang, Y.; Zhang, W. Influence of haunching on the static characteristics of high-speed railway box-type subgrade. *Railw. Stand. Des.* **2024**, *68*, 68–73.
19. Zhang, P.; Xiong, H.; Wang, R. Measurements and numerical simulations for cast temperature field and early-age thermal stress in zero blocks of high-strength concrete box girders. *Adv. Mech. Eng.* **2022**, *14*, 168781322210915. [CrossRef]
20. Liu, J.; Zhou, W.; Cao, J.; Li, X.; Jin, Y.; Ye, Q.; Feng, G. Dynamic performance of a slab track–concrete box subgrade under a double-line high-speed railway. *PLoS ONE* **2024**, *19*, e0311969. [CrossRef]
21. Chen, Y.; Xiao, H.; Song, X.; Guo, S.; Luo, B.; Nadakatti, M.M. Seismic response analysis of concrete box-type subgrade in high-speed railways. *Appl. Sci.* **2024**, *14*, 11899. [CrossRef]
22. Zhu, Z.; Qin, Y.; Wang, K.; Gong, W.; Zheng, W. Determination of settlement limit values for a new concrete box subgrade with ballasted track. *Structures* **2022**, *45*, 1646–1656. [CrossRef]
23. Wang, Z.; Huang, Q.; Xie, Q.; Xue, L.; Kang, X.; Gou, Y. Model test study on the dynamic response of high-speed railway subgrade crossing ground fissure zone. *Front. Earth Sci.* **2023**, *11*, 1113718. [CrossRef]
24. Chen, Y.; Xiao, H.; Guo, S.; Zhao, W.; Nadakatti, M.M.; Xu, A. Multi-objective optimization of structural parameters for new box-type subgrade based on genetic algorithm. *KSCE J. Civ. Eng.* **2025**, 100356, *in press*. [CrossRef]
25. Liu, J.; Liu, J.; Zhou, W.; Xia, B.; Zhang, Y.; Zhang, B.; Zhang, W. Study on static characteristics of optimized structure with haunch angle in box subgrade of high-speed railway. *Railw. Stand. Des.* **2024**, *68*, 68–73. [CrossRef]
26. Long, Y.; Bao, S. *Introduction to Structural Mechanics (I)*; Higher Education Press: Beijing, China, 2000; ISBN 7-04-001089-5.
27. *GB 50010-2010*; Code for Design of Concrete Structures. China Architecture & Building Press: Beijing, China, 2011.
28. Wang, J.; Tang, S.; Zheng, H.; Zhou, C.; Zhu, M. Flexural Behavior of a 30-Meter Full-Scale Simply Supported Prestressed Concrete Box Girder. *Appl. Sci.* **2020**, *10*, 3076. [CrossRef]
29. Liu, X. Research and Application of Modeling Pedi Rework of Domestic EMU. Master's Thesis, Southwest Jiaotong University, Chengdu, China, 2021.
30. *China CRH EMU*; Railway Engineering: Beijing, China, 2012; p. 106.
31. Liu, Y.-C.; Day, M.L. Simplified modelling of thin-walled box section beam. *Int. J. Crashworthiness* **2006**, *11*, 263–272. [CrossRef]
32. Liu, Y.; Day, M.L. Simplified modeling of cross members in vehicle design. In *Non-Conference Specific Technical Paper*; SAE International: Warrendale, PA, USA, 2007. [CrossRef]

Disclaimer/Publisher's Note: The statements, opinions and data contained in all publications are solely those of the individual author(s) and contributor(s) and not of MDPI and/or the editor(s). MDPI and/or the editor(s) disclaim responsibility for any injury to people or property resulting from any ideas, methods, instructions or products referred to in the content.